PAPER

A novel biomimetic dandelion structure-inspired carbon nanotube coating with sulfur as a lithium–sulfur battery cathode

View the article online for updates and enhancements.

Recent citations

A novel biomimetic dandelion structure-inspired carbon nanotube coating with sulfur as a lithium–sulfur battery cathode

Jinyun Liu[1] ⬤ , **Wen Zhang**[1] , **Yu Chen**[1] , **Ping Zhou**[2,3] **and Kaisheng Zhang**[2,3]

[1] Key Laboratory of Functional Molecular Solids, Ministry of Education, College of Chemistry and Materials Science, Anhui Normal University, Wuhu, Anhui 241002, People's Republic of China
[2] Institute of Intelligent Machines, Chinese Academy of Sciences, Hefei, Anhui 230031, People's Republic of China
[3] Department of Chemistry, University of Science and Technology of China, Hefei, Anhui 230026, People's Republic of China

E-mail: jyliu@iim.ac.cn

CrossMark

Abstract

Lithium–sulfur (Li–S) batteries have attracted considerable attention because of their high theoretical energy density. However, poor conductivity and a large volume change in S during cycling, together with a shuttle effect of polysulfides, severely restrict the battery performance, and remain a great challenge. Herein, inspired by a natural dandelion structure, we present a novel biomimetic S-coated carbon nanotube composite consisting of dandelion-like three-dimensional carbon nanotubes coated with S particles on the surface. Carbon nanotubes provide high-speed electron transfer pathways for S during cycling, while the special dandelion-like morphology provides a suitable environment for accommodating the volume change in S upon charge–discharge. The dandelion-like S-coated carbon nanotube-based Li–S batteries exhibit a stable capacity exceeding 760 mAh g^{-1} after 500 cycles at 0.1 C, along with a Coulombic efficiency as high as 99.9%. Even under repeated rounds of rate-performance measurements, and cycling at different charge versus discharge rates, the batteries retain high capacities and good recovery capabilities. In addition, the proportion of capacitive contribution in the overall capacity is high, indicating a good reversible capacity provided by the composite.

Supplementary material for this article is available online

Keywords: Li-S battery, biomimetic, nanocomposite, capacity

(Some figures may appear in colour only in the online journal)

1. Introduction

High energy density secondary batteries are in high demand for many applications, such as long driving range electric vehicles. Lithium–sulfur (Li–S) batteries have attracted extensive interest owing to their high theoretical energy density of 2600 Wh kg^{-1} [1–3]. However, since S is a molecular crystal, it possesses a poor electric conductivity of 5×10^{-30} S cm^{-1} [4, 5]. Moreover, S exhibits a large volume expansion (~80%) during discharge [6], leading to electrode cracks and damage. Improving the conductivity and

alleviating the volume change in S are important. Among many potential strategies, fabricating core–shell structures by coating a conductive layer on S, or loading S onto conductive substrates have been widely investigated to increase the conductivity [7]. For example, Chai *et al* prepared a graphene-embedded carbon fiber film which served as a conductive interlayer to improve the capacity retention and rate capability [8]. Geng's group used Na$_2$S/glucose as a template for constructing porous and conductive frames, which achieved a high content of S and good performance [9]. Su *et al* reported that nitrogen-doping generated defects and

active sites, leading to an improved electric property [10]. Zheng's group synthesized porous titanium nitride (TiN) tubes as an S host to improve the conductivity [11]. A Se/C-rich core–shell composite prepared by Zhang *et al* exhibited a discharge capacity of $558 \, \text{mAh g}^{-1}$ in the first cycle and remained at $181 \, \text{mAh g}^{-1}$ after 80 cycles at a rate of 0.5 C [12]. These achievements have demonstrated the advances in core–shell and frame-supported structures for constructing conductive and stable S cathodes. However, with regards to other issues, such as the volume change in S and the shuttle effect of polysulfides, emerging and optimal electrode structures are still highly desired.

To accommodate the volume change in S during cycling, the construction of three-dimensional (3D) porous nanostructures is considered promising [13, 14]. For example, Wang *et al* reported a self-supported 3D N-doped graphene foam, which was directly used as a binder-free electrode [15]. Li *et al* synthesized a 3D porous graphene aerogel through a modified two-step hydrothermal reduction route, which possessed good electric conductivity [16]. A nickel phosphide nanoporous composite derived from metal-organic frameworks (MOFs) was prepared as the S host by Sun's group, which exhibited accelerated electron transportation [17]. Moreover, Liang *et al* reported a nitrogen-doped carbon nanofiber with a 3D interconnected pore structure, which was beneficial for enhancing the adsorption of polysulfides and buffering the volume expansion of S [18]. These efforts have shown their potential to achieve an appropriate environment for accommodating the volume change in S. Nevertheless, it remains a great challenge to simultaneously address the conductivity and volume change issues.

Recently, biomimetic structures have been introduced to the research communities of nanomaterial and nanotechnology, including batteries, sensors, etc [19–22]. Dai *et al* fabricated a conductive honeycomb-like cathode consisting of metallic and polar Co_9S_8 tubes [23]. The biomimetic structure is able to bind the polysulfides, achieving a prolonged cycle life. Wang *et al* reported a pomegranate-like microcluster, which delivered a capacity of $650 \, \text{mAh g}^{-1}$ after 400 cycles at 1 C [24]. A cabbage-like nitrogen-doped graphene/S composite with good capacity was made by Cui *et al* [25]. In addition, it was confirmed that root-like porous carbon nanofibers could accommodate the volume expansion [26]. Since then, it is possible to address the conductivity and volume change issues by fabricating biomimetically-structured electrode materials.

As is known, the natural dandelion is a 3D radial sphere consisting of numerous rod-like seeds assembling on the core. Such a special 3D porous morphology enables each seed to contact with the surrounding moisture and sunlight efficiently. Inspired by this, herein, we present a unique biomimetic S-coated carbon nanotube composite consisting of dandelion-like 3D radial carbon nanotubes loaded with S particles. Within this composite, the carbon nanotubes provide high-speed electron transfer pathways for S during cycling. The special 3D porous dandelion-like morphology enables a suitable environment for accommodating the volume change in S upon charge–discharge. As illustrated in figure 1(a), 3D ZnO nanorods as a template were synthesized through a hydrothermal route. Then, a carbon layer was coated on the surface of ZnO through *in situ* polymerization and subsequent thermal treatment. After removing the ZnO nanorods by acid etching, hollow 3D radial carbon nanotubes were formed. Finally, the S particles were loaded onto the carbon tubes on the basis of a sublimation-adsorption-condensing mechanism, forming a 3D S-coated carbon nanotube composite with a biomimetic dandelion-like structure. The composite exhibits a good capacity and cycling stability. The capacities exceed 760 and $615 \, \text{mAh g}^{-1}$ after 500 cycles at 0.1 C and 800 cycles at 0.5 C, respectively.

## 2. Experimental

2.1. Preparation of 3D ZnO nanorods

The 3D ZnO nanorods used as a template for constructing the carbon nanotubes were prepared through a hydrothermal route. Typically, 2.24 g of KOH (Sinopharm Chemical Reagent Co. Ltd) was dissolved in 10 ml of deionized water, forming a solution denoted as solution A. Then, 1.48 g of $Zn(NO_3)_2 \cdot 6H_2O$ (Sinopharm Chemical Reagent Co. Ltd) was dissolved in 10 ml of deionized water as solution B. Solution B was dropped into A under constant stirring. The solution was heated at 50 °C for 6 h. The resulting precipitate was collected and washed with deionized water and ethanol. Finally, the samples were dried at 60 °C in an oven.

2.2. Preparation of carbon-coated ZnO nanorods

First, a carbon layer was coated on the ZnO nanorods; 0.2 g of the ZnO was dispersed in 50 ml of deionized water by ultrasonication for 15 min. Then, 1.211 g of tris (hydroxymethyl) aminomethane (Aladdin Reagent Shanghai Co. Ltd) was added to the solution under stirring. Then, 200 μl of concentrated hydrochloric acid was added. Next, 75 mg of dopamine hydrochloride (Aladdin Reagent Shanghai Co. Ltd) was added under stirring. The solution was stirred for 24 h. The product was collected, washed with deionized water and ethanol alternately, and dried in an oven at 60 °C for 6 h. The sample was calcined at 550 °C for 5 h in a nitrogen gas flow at a ramping rate of $2 \, °\text{C} \, \text{min}^{-1}$. Finally, hollow carbon tubes were prepared by removing the ZnO core by immersing in 20 ml of 0.5 M HCl solution for 20 min. The samples were washed with deionized water and ethanol, and dried at 60 °C.

2.3. Preparation of dandelion-like S-coated carbon nanotubes

Typically, 0.1 g of the as-obtained 3D carbon nanotubes and 0.2 g of S powders (Aladdin Reagent Shanghai Co. Ltd) were mixed and transferred into a polytetrafluoroethylene bottle, which was then filled with Ar gas, operated in an Ar-filled glove box. The bottle was sealed tightly, then put into an oven at 140 °C for 14 h. After the bottle completely cooled down naturally, the S-coated carbon nanotubes were collected.
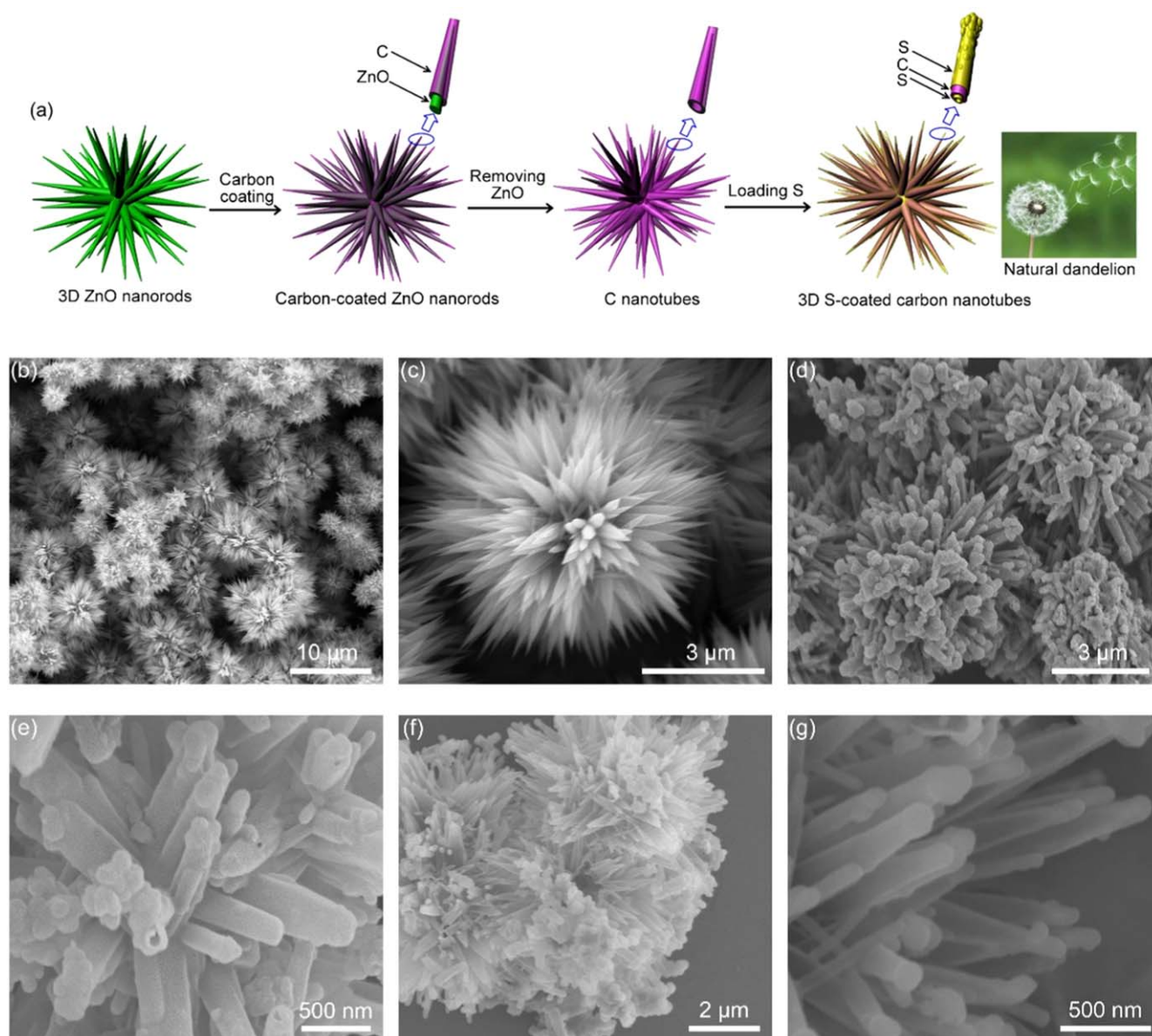
Figure 1. (a) A schematic illustration of the formation process of dandelion-like S-coated carbon nanotubes. SEM images of (b), (c) 3D ZnO nanorods, (d) carbon-coated ZnO, (e) carbon nanotubes after ZnO removal, and the (f), (g) S-coated carbon nanotubes.

2.4. Characterization

The samples were characterized using x-ray diffraction (XRD, Shimadzu XRD-6000) with Cu Kα radiation at a wavelength of 1.5418 Å, field emission scanning electron microscopy (FESEM, Hitachi S-4800, operated at 5 kV), transmission electron microscopy (TEM, JEOL-2010 TEM with an acceleration voltage of 200 KV), x-ray photoelectron spectroscopy (XPS, ESCALAB 250) and Raman spectroscopy (Renishaw inVia) with a laser of 532 nm. Energy dispersive spectroscopy (EDS) and elemental mappings were carried out on the same FESEM operated at 15 kV. Thermogravimetric analysis (TGA) was performed on a Setaram Labsys Evo SDT Q600 at a heating rate of 10 °C min^{-1} from room temperature to 800 °C in an air flow. The Brunauer–Emmett–Teller (BET) surface area and pore-size distribution of the 3D carbon nanotubes were measured

on a Coulter Omnisorp 100CX instrument using N$_2$ adsorption–desorption.

2.5. Electrochemical measurements

The electrochemical properties of the prepared dandelion-like 3D S-coated carbon nanotube composite were evaluated as cathodes in Li–S batteries using a coin cell system. The cathodes were fabricated using the composite (70 wt%), carbon black (20 wt%) and polyvinylidene fluoride binder (10 wt%) in N-methylpyrrolidone. The mixture was mixed into a homogeneous slurry and uniformly coated onto a 14 mm-diameter and 0.015 mm thick aluminum foil (Aladdin Reagent Shanghai Co. Ltd), and dried in a vacuum at 60 °C for 12 h. The loading of the S in the electrode was about 3.2 mg cm^{-2}. The batteries were fabricated in an Ar-filled glove box (O$_2$ level < 0.01 ppm, H$_2$O level<0.01 ppm,

Mikrouna, Super 1220/750/900). The Li foil (Aladdin Reagent Shanghai Co. Ltd) was used as the counter/reference electrode. The electrolyte was 1 M bis (trifluoromethane) sulfonamide lithium salt (LiTFSI, Sigma Aldrich) in a mixed solvent of 1,3-dioxolane and 1,2-dimethoxyethane at a volume ratio of 1:1. The galvanostatic discharge-charge tests were performed at a potential window of 1.7 to 2.8 V on a Neware battery-testing system (Neware CT-3008). Cyclic voltammetry (CV) profiles were recorded on an electro-chemical workstation (Huachen CHI-660E). Electrochemical impedance spectroscopy (EIS) was recorded over the range of 0.01–100 kHz on the same electrochemical workstation.

3. Results and discussion

The morphology and structure of the samples during fabri-cation are shown in figures 1(b)–(g). In figure 1(b), the ZnO nanorods assemble as a spherical sphere at a size of 5–8 μm. As seen from the zoomed-in SEM image (figure 1(c)), there are numerous ZnO nanorods growing on the core, showing a 3D radial morphology. Figure 1(d) displays the SEM image of the carbon-coated ZnO nanorods. Compared to the pristine ZnO nanorods, the ZnO coated with carbon retains a dande-lion-like structure while the surface becomes obviously rough, indicating the coating of carbon. After the acid treat-ment was employed to remove the ZnO core, hollow carbon tubes were obtained, as shown in figure 1(e). It is noted that through BET surface area and pore-size distribution mea-surements, meso-pores at a dominating size of about 5 nm were confirmed, as shown in figure S1 in the online supple-mentary information, available at stacks.iop.org/NANO/30/155401/mmedia. The pores enable the penetration of acid through the carbon wall, and thus etching of the ZnO core. Such a 3D tubular structure would not only facilitate the volume change in electrochemically-active materials in charge–discharge, but is also beneficial for the electrolyte diffusion throughout the entire electrode. Figures 1(f) and (g) show the SEM image of the 3D S-coated carbon nanotube composite after loading S onto carbon. The dandelion-like structure remains well, indicating a robust mechanical strength. Each nanotube assembles at one end while showing radially along the tip, and a number of voids remain among the tubes, which provide efficient spaces for accommodating the volume change in S during cycling.

The XRD pattern of the as-prepared composite is dis-played in figure 2. All the diffraction peaks are in good agreement with the S in a Joint Committee on Powder Dif-fraction Standards (JCPDS) card no. 08-0247. The strong intensity of the diffraction peaks indicates a high loading of S within the composite, which will be confirmed using TGA below. In addition, no signal from impurity was detected, confirming a high purity. Figures 3(a) and (b) display the TEM images of the 3D carbon nanotubes. After etching with an acid solution, the ZnO nanorods were removed com-pletely, forming a hollow structure. The diameter of the nanotubes is about 300 to 400 nm, while the wall of the nanotubes is about 90 nm in thickness. The TEM images of
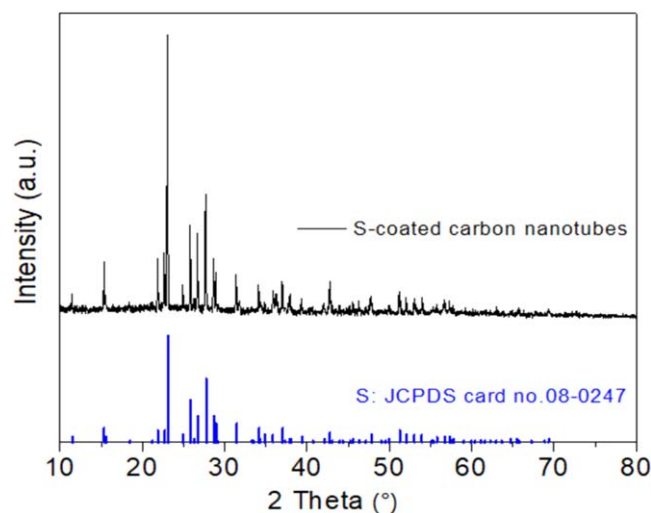

Figure 2. An XRD pattern of the dandelion-like S-coated carbon nanotubes. The lines at the bottom indicate the peak information of S in a JCPDS card (no. 08-0247).

the 3D S-coated carbon nanotubes are shown in figures 3(c) and (d). The dandelion-like morphology is confirmed. Similar to the SEM images shown above (figures 1(f) and (g)), the wall of the nanotubes is obviously rough, exhibiting dense particles on the tubes. Another point of interest is that the tip of each tube is rougher than the other end on the core, indi-cating that more S particles are at the tips. This is ascribed to the minimum surface energy theory that the sharp angle possesses a higher surface energy than the planar region, which makes more S be adsorbed and condensed at the tips [27–29].

Figure 4(a) shows the SEM image of the S-coated carbon nanotubes. Figures 4(b) and (c) display the mapping images. The uniform distribution of the C and S elements throughout the composite is observed. Figure 4(d) shows the EDS spectrum, which confirms the elements of the composite. To demonstrate the composition of the composite, XPS spectra were measured, as shown in figure 5. In the survey spectrum (figure 5(a)), the presence of elements C and S without impurities is confirmed. Figure 5(b) displays the XPS spec-trum of S 2p in which the peaks at 163.8 and 165.0 eV are assigned to S $2p_{3/2}$ and S $2p_{1/2}$, respectively [30]. The peak at about 169.2 eV is ascribed to the sulfate species formed by the oxidation of sulfur in air [31, 32]. In figure 5(c), the spectrum of C 1s was divided into three parts with peaks at 284.7, 285.6, and 288.4 eV, which are assigned to C–C/C=C, C–O/C–S, and O–C=O, respectively [33, 34].
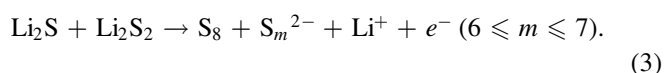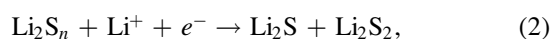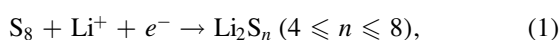
Figure 6(a) displays the Raman spectra of the 3D carbon nanotubes and the S-coated carbon nanotube composite. There are two broad peaks at 1594.9 and 1357.9 cm^{-1}, which correspond to a graphite carbon layer-like graphite band (G band) and a carbon disordered disorder band (D band), respectively [35]. The intensity ratio (I_D/I_G) of the D and G bands of the carbon nanotubes is about 0.91, which is close to the ratio of the composite (0.88), indicating that the loading of S does not impact the carbon structure. This is beneficial for
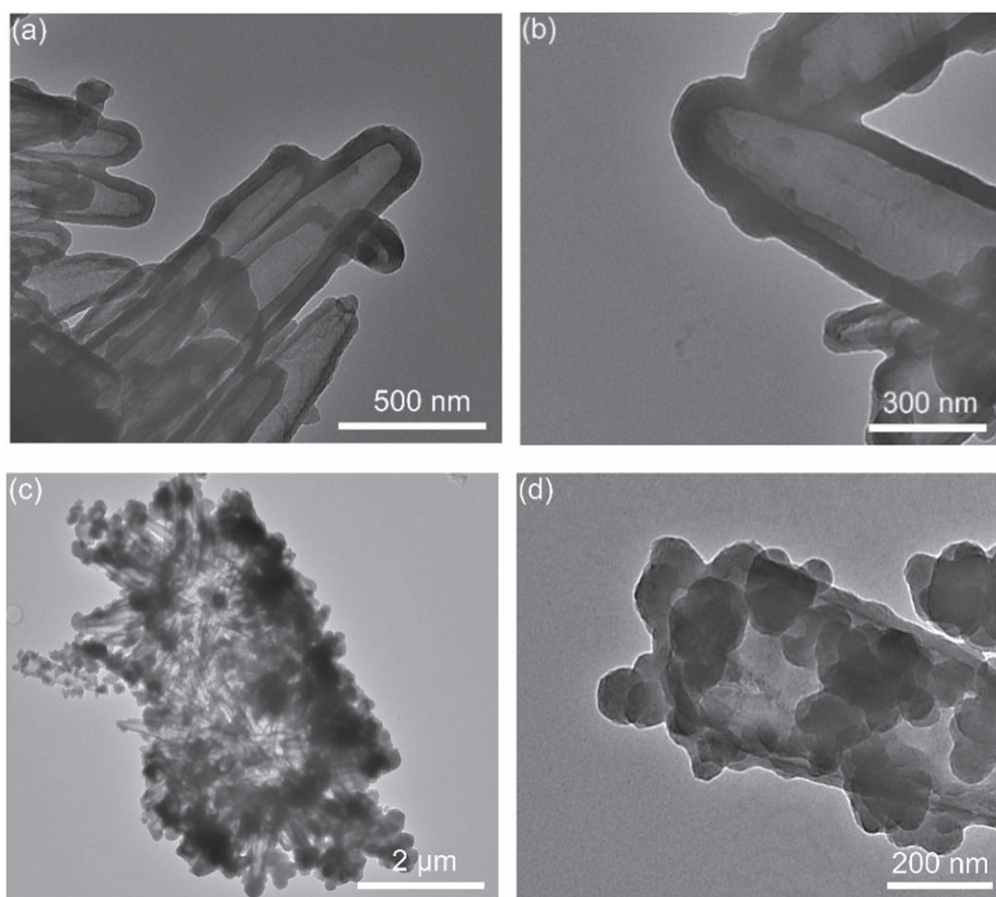
Figure 3. TEM images of the (a), (b) carbon nanotubes, and the (c), (d) 3D S-coated carbon nanotube composite.

retaining good conductivity of the carbon nanotubes. In addition, to determine the content of S in the composite, TGA was conducted, as shown in figure 6(b). As seen, the curves of the commercial S powders and the S-coated carbon nanotubes show an obvious weight loss from 120 °C to 300 °C, which is ascribed to the sublimation of S. The TGA profile of the composite exhibits an additional weight loss from 400 °C, which is assigned to the oxidation of carbon. Calculated from the TGA curves, the content of S in the dandelion-like composite is about 73.2%, which indicates that the loading of S is competitive, compared to some reported S-based composites [36–38].

Figure 7 displays the electrochemical performance of the dandelion-like S-coated carbon nanotube composite. The galvanostatic charge–discharge curves cycling at 0.1 C (1 C equivalent to 1 h full charge or discharge to a sulfur theoretical capacity of 1675 mAh g^{-1}) is shown in figure 7(a). Two obvious plateaus at approximately 2.1 and 2.3 V during discharge, and one plateau at 2.35 V during charge are observed. The electrochemical reactions can be presented as follows [9, 39]:

$$S_8 + Li^+ + e^- \rightarrow Li_2S_n \ (4 \leqslant n \leqslant 8), \tag{1}$$

$$Li_2S_n + Li^+ + e^- \rightarrow Li_2S + Li_2S_2, \tag{2}$$

$$Li_2S + Li_2S_2 \rightarrow S_8 + S_m^{2-} + Li^+ + e^- \ (6 \leqslant m \leqslant 7). \tag{3}$$

The plateau at 2.3 V corresponds to the conversion process of the S_8 ring opening and the long-chain polysulfide ion Li_2S_n ($4 \leqslant n \leqslant 8$). The one at 2.1 V is assigned to the process of reducing Li_2S_n to Li_2S_2/Li_2S [40–43]. In contrast, an oxidation plateau appearing at about 2.35 V corresponds to the conversion of Li_2S to Li_2S_8 during charge. As seen from figures 7(a) and (b), after cycling at 0.1 C for 500 times, the composite retains a stable capacity of 760 mAh g^{-1}, along with a Coulombic efficiency of ≈99.9%, showing a good reversibility. As the control experiment, the battery based on the commercial S powder cathode exhibits an obviously lower capacity of about 300 mAh g^{-1} after 250 cycles at 0.1 C along with an unstable Coulombic efficiency, as shown in figure S2. The CV curves obtained at a scanning rate of 0.1 mV s^{-1} is shown in figure 7(c). There are two reduction peaks located near 2.1 and 2.3 V, respectively, which are consistent with the discharge plateaus in figure 7(a). To further investigate the stability of the composite, the batteries were cycled at a relatively large rate of 0.5 C, as shown in figures 7(d) and S3. After cycling at 0.5 C for 800 times, the capacity remians above 615 mAh g^{-1}, along with a capacity decay rate less than 0.9% per cycle. In contrast, the battery consisting of commercial S powder-based cathodes shows a low capacity less than 200 mAh g^{-1} after 700 cycles. The capacity of the composite decays obviously during the initial period, which is ascribed to the loss of active S on the top layer. Upon
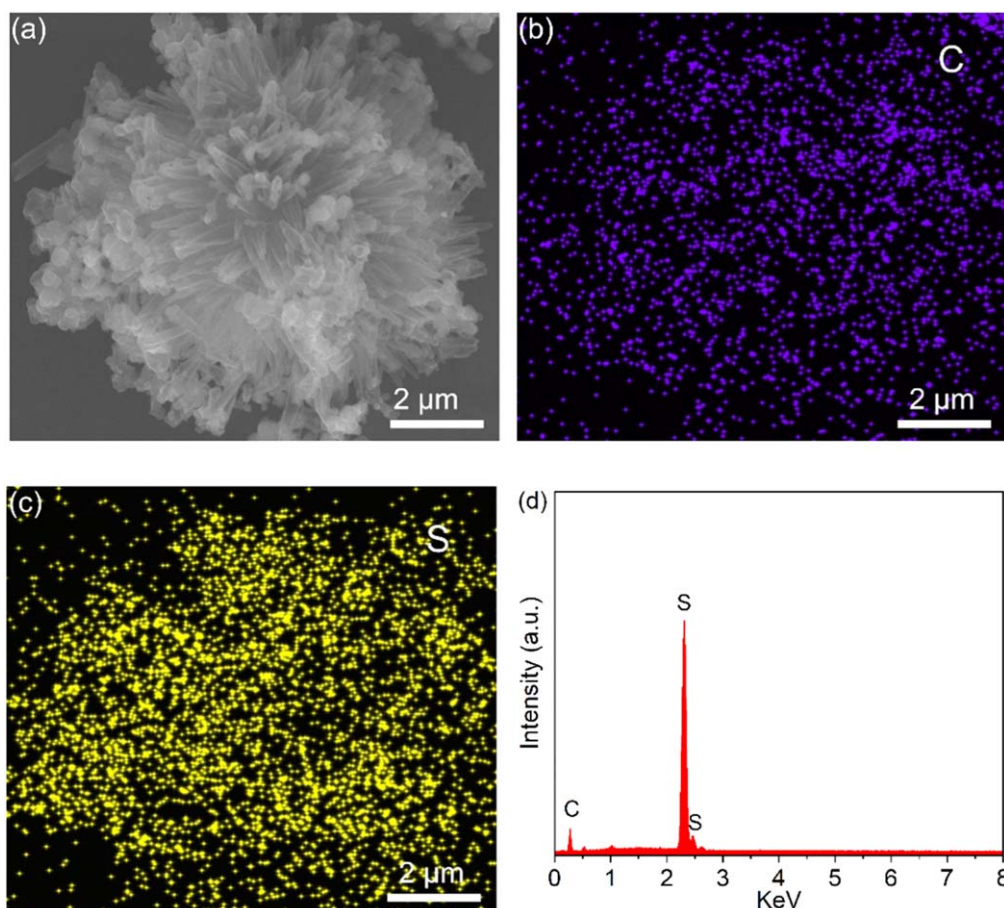
Figure 4. (a) The SEM image, and the elemental mappings of (b) C, (c) S and (d) the EDX spectrum.
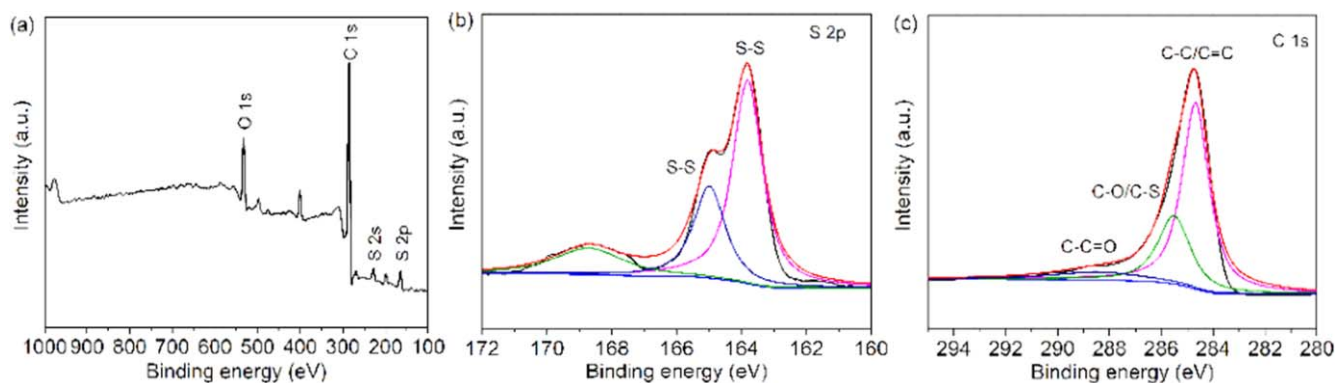

Figure 5. (a) The survey XPS spectrum, (b) S 2p, and (c) C 1s spectra of the S-coated carbon nanotubes.

lithiation, the volume of S expands, leading to a poor adherence with the carbon tubes. In contrast, the S near the carbon surface would play a dominating role in contributing the capacity during the subsequent cycles. The meso-porous carbon nanotubes are able to adsorb the S and polysulfides, and thus improve the stability of the capacity during the subsequent cycles. The capacity of the S powders is low, which is ascribed to the large size and the poor conductivity. The SEM images of the S powders (figure S4), display a size of about 5 μm. The large size makes it unable to efficiently accommodate the volume change in S during cycling; while

the poor conductivity, which will be confirmed below through EIS spectra, indicates that the internal part of S can hardly be utilized for reacting with Li ions, leading to a low capacity compared to the theoretical value.

The rate performance of the S-coated carbon nanotubes is shown in figures 8(a) and (b). The battery exhibits stable capacities at 0.05 C, 0.1 C, 0.2 C, 0.5 C and 1 C, which are 1090, 890, 820, 730 and 680 mAh g^{-1}, respectively. Once the cycling rate was turned back to 0.05 C, the capacity recovered to 880 mAh g^{-1}. As seen in figure 8(b), even after a second round of rate-performance measurement, the capacities remain stable. In
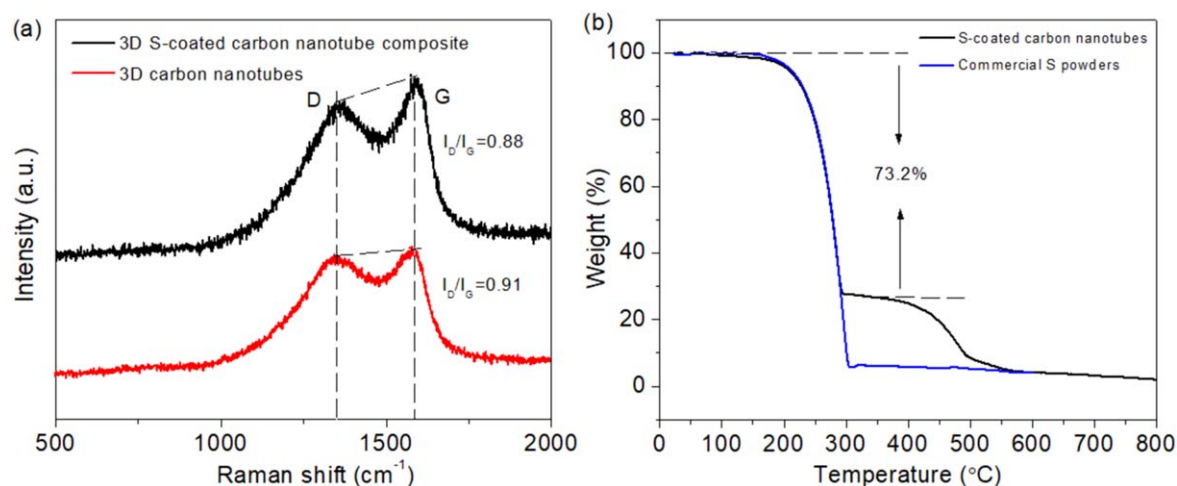
Figure 6. (a) Raman spectra of the S-coated carbon nanotube composite and the 3D carbon nanotubes; and (b) TGA curves of the composite and commercial S powders.
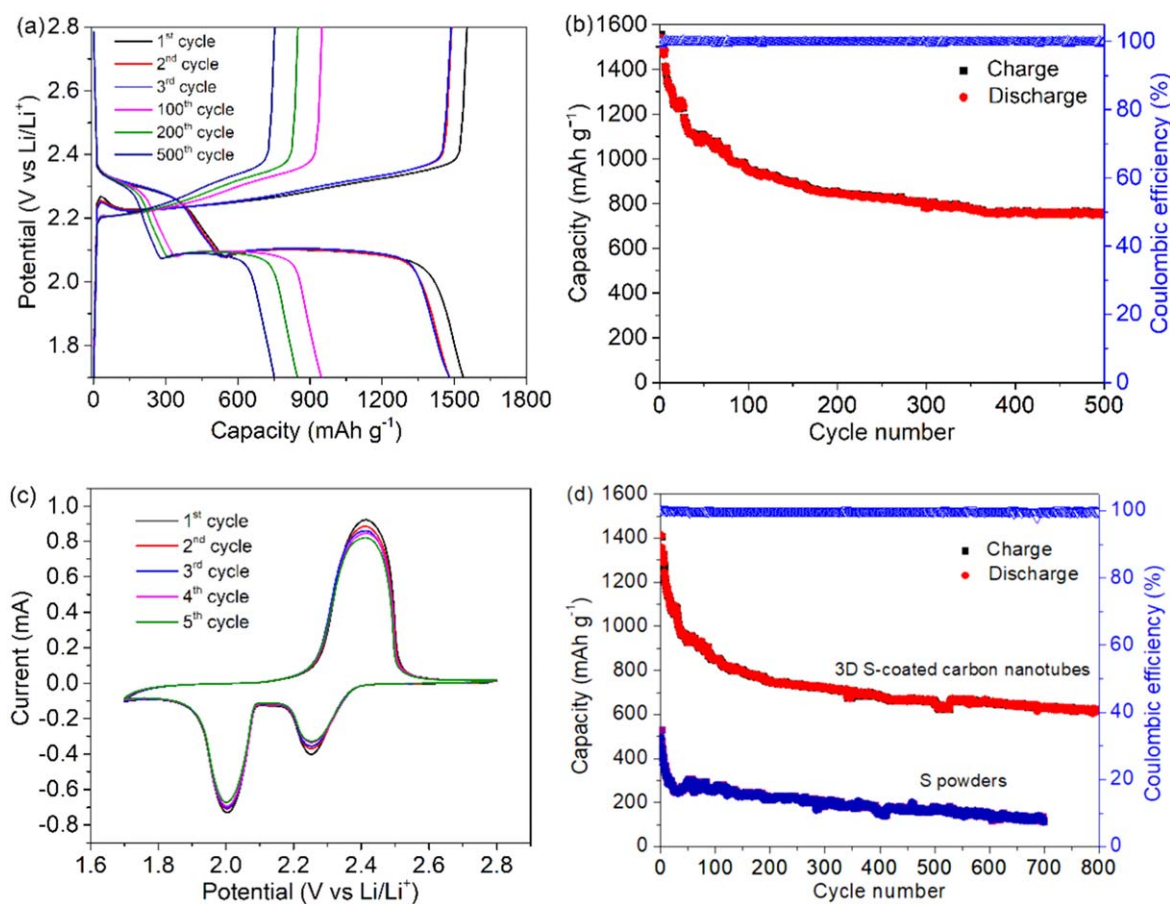

Figure 7. (a) The charge–discharge curves and (b) capacity and Coulombic efficiency of the 3D S-coated carbon nanotubes cycling at the potential window of 1.7–2.8 V at 0.1 C. (c) CV curves at a scanning rate of 0.1 mV s^{-1}. (d) Capacity and Coulombic efficiency of the S-coated carbon nanotube composite and S powders cycling at 0.5 C.

addition, as shown in figures 8(c) and (d), when charging at 0.2 C and discharging at 0.4 C, or the reverse, the capacities exhibit a good stability and a high Coulombic efficiency, particularly after the initial ten cycles. The good rate performance is ascribed to the rapid electron transfer provided by the conductive carbon nanotubes, and the special 3D biomimetic dandelion-like structure,

which is appropriate for electrolyte infiltration and Li$^+$ ion diffusion. The EIS spectra of the S-coated carbon tube composite and the commercial S powders are displayed in figure S5. Both of the spectra consist of a semicircle at the mid-high frequency and a diagonal line at the low frequency. The semicircle at the intermediate frequency is approximately equal to the charge
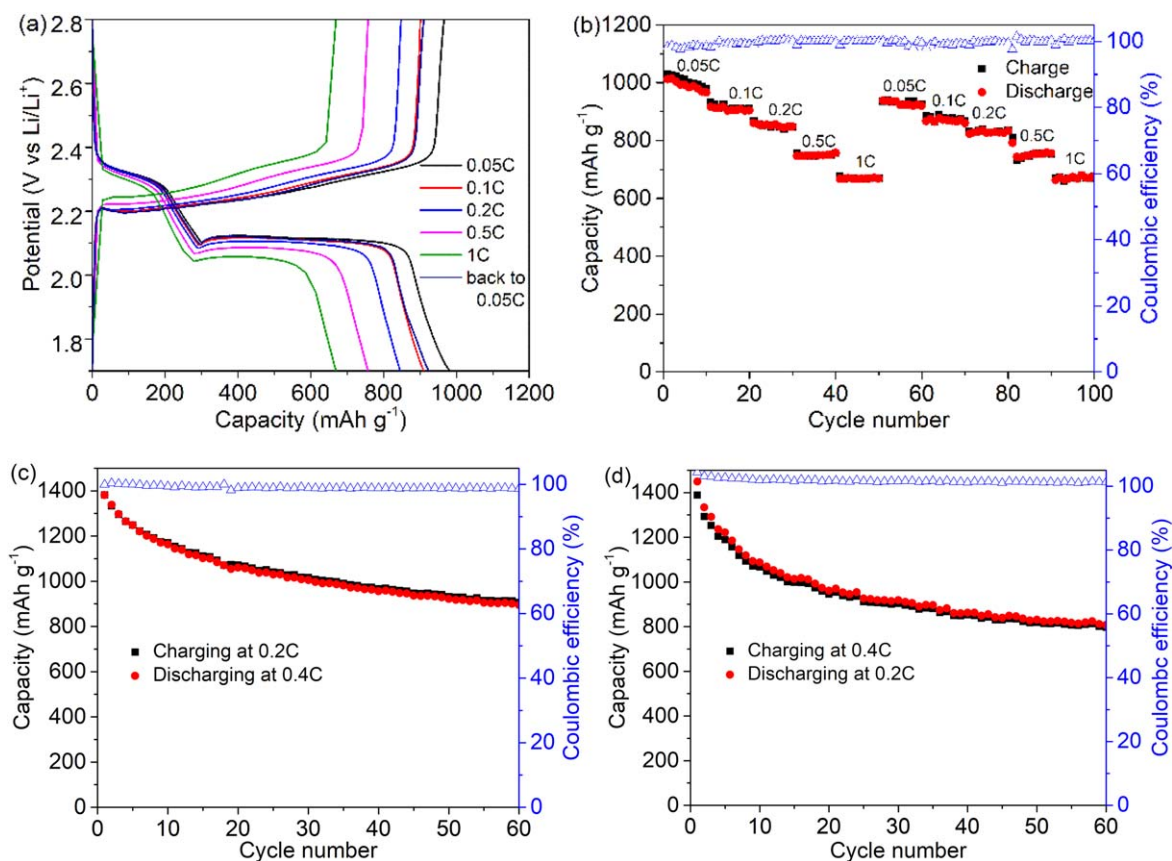
Figure 8. (a) Charge–discharge profiles and (b) rate performance of the dandelion-like S-coated carbon nanotubes. Cycling performance at (c) a charge rate of 0.2 C and a discharge rate of 0.4 C, and (d) at a charge rate of 0.4 C and a discharge rate of 0.2 C.

Table 1. A comparison of the cycling performance of some S composites.

Materials	Preparation method	Cycling rate	Cycle number	Capacity (mAh g^{-1})	Reference
Carbon nanofiber/S	S infusion	0.5 C	150	630	[3]
3D porous Se/S/C	Melting-diffusion method	0.5 A g^{-1}	200	486	[4]
Core–shell S@MnO$_2$	Hydrothermal route	0.5 C	800	480	[14]
rGO/S/polyaniline	Hydrothermal route	0.1 C	100	600	[42]
N-doped porous carbon@S	Hydrothermal route	0.1 C	500	636	[44]
Porous graphitic carbon nitride/S	Hydrothermal route	0.2 C	500	620	[6]
Metal-organic framework@rGO/S	Two-step liquid phase method	335 mA g^{-1}	50	650	[39]
CNT/S@polypyrrole	Electrodeposition	0.2 C	100	617	[32]
MoS$_2$/rGO/S	Melt-diffusion method	0.5 C	200	680	[45]
Acetylene black/S@polypyrrole	*In situ* S deposition method	0.5 C	200	454	[46]
Sulfur/polypyrrole tubular composite	One-pot synthesis	0.2 C	200	692	[47]
Nitrogen-enriched porous carbons@S	Melt-diffusion method	0.2 C	100	758	[48]
C/S@polypyrrole	*In situ* chemical oxidative polymerization	1 C	60	400	[49]
Dandelion-like S-coated carbon nanotube composite	Templated preparation	0.1 C	500	760	This work
		0.5 C	800	615	

transfer resistance (R_{ct}). The semicircle size of the S-coated carbon tube composite is much less than that of the S powders, indicating a lower charge transfer resistance. Through calculations, the resistances for the composite and the S powders are about 31

and 112 Ω, respectively. In addition, a comparison of the cycling performance with other S-based composites is listed in table 1, which indicates that the presented dandelion-like S-coated carbon nanotubes demonstrate a competitive performance.
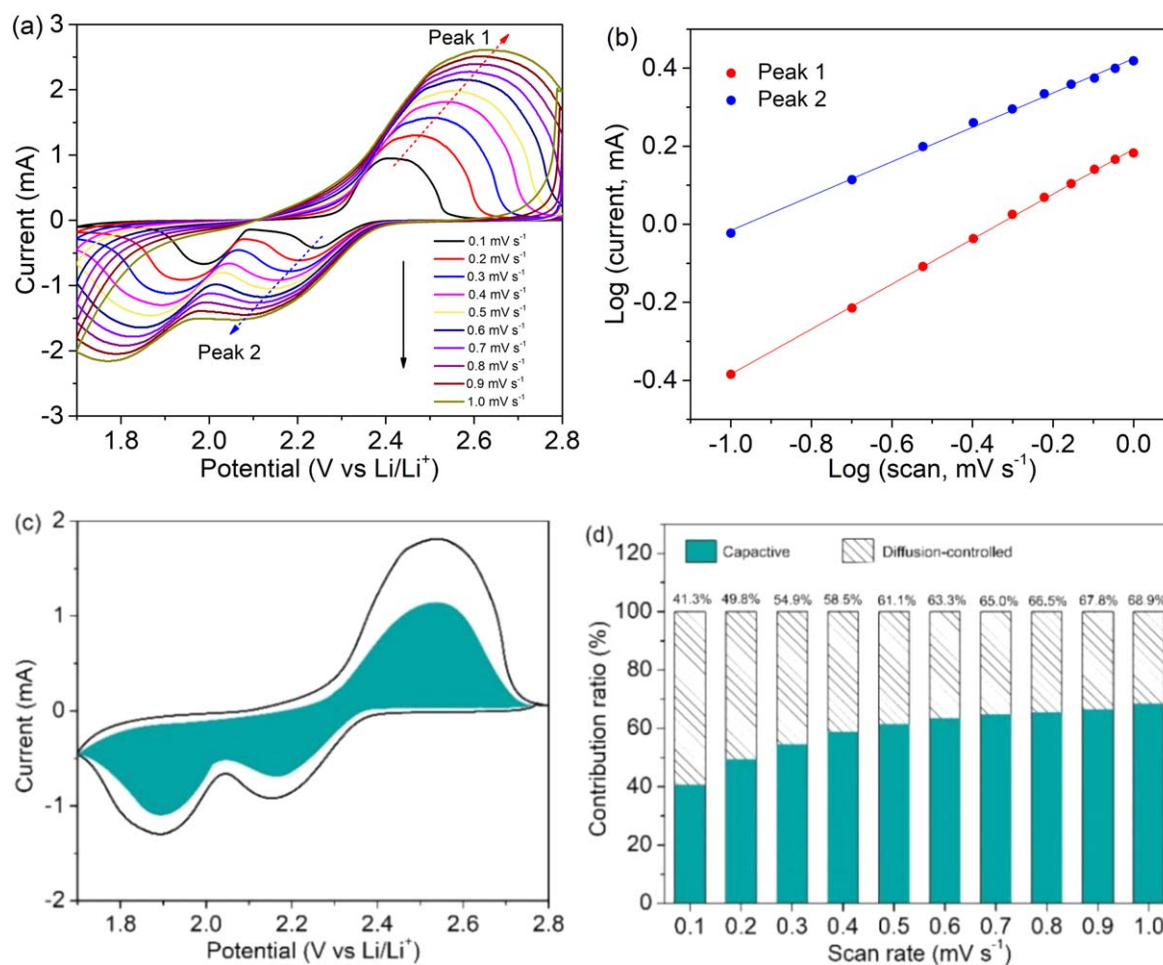
Figure 9. (a) CV curves of the S-coated carbon nanotube composite at a series of scanning rates, (b) the profile of log(i) versus log(v), (c) the capacitive contribution in a CV profile of 0.5 mV s^{-1}, (d) the contribution ratio of capacitive and diffusion-controlled charge at different rates.

The CV curves at a series of scanning rates from 0.1 to 1.0 mV s^{-1} were also investigated, as displayed in figure 9(a). As known, the current (i) obeys a power law with respect to the scanning rate (v) by following the equation: $i(v) = av^b$. It represents a diffusion-controlled process when b is 0.5; while it is ideally capacitive when b is 1 [50, 51]. Both a and b can be determined by the slope and intercept from figure 9(b). In the range of 0.1 to 1.0 mV s^{-1}, the b values for cathodic and anodic peaks are 0.44 and 0.57, respectively, indicating a kinetic diffusion-controlled behavior. The capacity contributions from capacitive and diffusion-controlled charge could be quantified on the basis of the relationship: $i(v) = k_1v + k_2v^{1/2}$, where k_1v and $k_2v^{1/2}$ correspond to the current contributions from the surface capacitive effects and the diffusion-controlled intercalation process, respectively [52]. As a demonstrating example, the shaded region in figure 9(c) shows the capacitive contribution at 0.5 mV s^{-1}. Figure 9(d) displays the capacity contribution at different scanning rates, which indicates that the percentage of capacitive contribution increases depending on the elevation of the scanning rates.

4. Conclusions

In summary, we present a novel biomimetic dandelion-like composite consisting of 3D carbon nanotubes coated with S particles, which exhibit good electrochemical performance as the cathode in a Li–S battery. The dandelion-like 3D S-coated carbon nanotube cathode retains a stable capacity of 760 mAh g^{-1} after cycling at 0.1 C for 500 times, and a capacity of 615 mAh g^{-1} after 800 cycles at 0.5 C along with a Coulombic efficiency above 99.8%. During repeated rounds of the rate-performance measurements, or cycling at different charge versus discharge rates, the batteries exhibit good cycling capacities and reversible capability. Compared to some reported S cathodes, the biomimetic structured composite is competitive. The improved performance is ascribed to the fact that the carbon nanotubes provide high-speed electron transfer pathways for S; and the dandelion-like structure enables efficient accommodation of the volume change in S during charge–discharge. It is expected that the biomimetically-structured electrode design is applicable for many secondary batteries. In addition, the general preparation approach will also be of interest to many research fields, such as energy storage, sensors, catalysts, etc.

ORCID iDs

Jinyun Liu ⓘ https://orcid.org/0000-0001-6619-3886

References

[1] Deng D R, Lei J, Xue F, Bai C D, Lin X D, Ye J C, Zheng M S and Dong Q F 2017 *In situ* preparation of a macro-chamber for S conversion reactions in lithium-sulfur batteries *J. Mater. Chem.* A **5** 23497–505

[2] Li C X, Gao K and Zhang Z P 2018 Graphitic carbon nitride as polysulfide anchor and barrier for improved lithium-sulfur batteries *Nanotechnology* **29** 465401

[3] Zheng G Y, Yang Y, Cha J J, Hong S S and Cui Y 2011 Hollow carbon nanofiber-encapsulated sulfur cathodes for high specific capacity rechargeable lithium batteries *Nano Lett.* **11** 4462–7

[4] Hu J, Zhong H, Yan X and Zhang L 2018 Confining selenium disulfide in 3D sulfur-doped mesoporous carbon for rechargeable lithium batteries *Appl. Surf. Sci.* **457** 705–11

[5] Liang C Y, Zhang X M, Zhao Y, Tan T Z, Zhang Y G and Bakenov Z 2018 Three-dimensionally ordered macro/ mesoporous TiO$_2$ matrix to immobilize sulfur for high performance lithium/sulfur batteries *Nanotechnology* **29** 415401

[6] Pang Q and Nazar L F 2016 Long-life and high-areal-capacity Li-S batteries enabled by a light-weight polar host with intrinsic polysulfide adsorption *ACS Nano* **10** 4111–8

[7] Peng H J, Huang J Q, Cheng X B and Zhang Q 2017 Review on high-loading and high-energy lithium-sulfur batteries *Adv. Energy Mater.* **7** 1700260

[8] Chai L, Wang J, Wang H, Zhang L, Yu W and Mai L Q 2015 Porous carbonized graphene-embedded fungus film as an interlayer for superior Li-S batteries *Nano Energy* **17** 224–32

[9] Li G X, Sun J H, Hou W P, Jiang S D, Huang Y and Geng J X 2106 Three-dimensional porous carbon composites containing high sulfur nanoparticle content for high-performance lithium-sulfur batteries *Nat. Commun.* **7** 10601

[10] Su D, Cortie M and Wang G 2017 Raman spectra of graphite oxide and functionalized graphene sheets *Adv. Energy Mater.* **7** 1602014

[11] Deng D R, An T H, Li Y J, Wu Q H, Zheng M S and Dong Q F 2016 Hollow porous titanium nitride tubes as a cathode electrode for extremely stable Li-S batteries *J. Mater. Chem.* A **4** 16184–90

[12] Zhang Z, Yang X, Guo Z, Qu Y, Li J and Lai Y 2015 Selenium/carbon-rich core–shell composites as cathode materials for rechargeable lithium-selenium battery *J. Powder Sources* **279** 88–93

[13] Mi L W, Xiao W D, Cui S Z, Hou H W and Chen W H 2016 An N-doped three dimensional flexible carbon/sulfur cathode for lithium sulfur battery design *Dalton Trans.* **8** 3305–9

[14] Liang X and Nazar L F 2016 *In situ* reactive assembly of scalable core–shell sulfur-MnO$_2$ composite cathodes *ACS Nano* **10** 4192–8

[15] Wang Y, Huang J, Chen X, Wang L and Ye Z 2018 Powder metallurgy template growth of 3D N-doped graphene foam as binder-free cathode for high-performance lithium/sulfur battery *Carbon* **137** 368–78

[16] Li B, Xiao Q and Luo Y 2018 A modified synthesis process of three-dimensional sulfur/graphene aerogel as binder-free cathode for lithium sulfur batteries *Mater. Design* **153** 9–14

[17] Cheng J, Zhao D, Fan L, Wu X, Wang M, Wu H, Guan B, Zhang N and Sun K 2018 A conductive Ni$_2$P nanoporous composite with 3D structure derived from metal-organic framework for lithium-sulfur batteries *Chem. Eur. J.* **24** 13253–8

[18] Liang Y, Deng N, Ju J, Zhou X, Yan J, Zhong C, Kang W and Cheng B 2018 Facilitation of lithium polysulfides adsorption by nitrogen doped carbon nanofibers with 3D interconnected pore structures for high-stable lithium-sulfur batteries *Electrochim. Acta* **281** 257–65

[19] Manoj M, Jasna M, Anilkumar K M, Abhilash A, Jinisha B, Pradeep V S and Jayalekshmi S 2018 Sulfur-polyaniline coated mesoporous carbon composite in combination with carbon nanotubes interlayer as a superior cathode assembly for high capacity lithium-sulfur cells *Appl. Surf. Sci.* **458** 751–61

[20] Wen X, Xiang K, Zhu Y, Xiao L, Chen X and Chen H 2018 Preparation of Mn$_3$O$_4$-CNTs microspheres as an improved sulfur hosts for lithium-sulfur batteries *Mater. Lett.* **229** 272–6

[21] Sun P, Cao Y, Liu J, Sun Y, Ma J and Lu G 2011 Dispersive SnO$_2$ nanosheets: hydrothermal synthesis and gas-sensing properties *Sens. Actuator* B **156** 779–83

[22] Li W Y, Liang Z, Lu Z D, Yao H B, Seh Z W, Yan K, Zheng G Y and Cui Y 2015 A sulfur cathode with pomegranate-like cluster structure *Adv. Energy Mater.* **5** 1500211

[23] Dai C *et al* 2018 Honeycomb-like spherical cathode host constructed from hollow metallic and polar Co$_9$S$_8$ tubules for advanced lithium-sulfur batteries *Adv. Funct. Mater.* **28** 1704443

[24] Wang P, Zhang Z, Yan X, Xu M, Chen Y, Li J, Li J, Zhang K and Lai Y 2018 Pomegranate-like microclusters organized by ultrafine Co nanoparticles@nitrogen-doped carbon subunits as sulfur hosts for long-life lithium-sulfur batteries *J. Mater. Chem.* A **6** 14178–87

[25] Cui Z, Mei T, Yao J, Hou B, Zhu X, Liu X and Wang X 2018 Cabbage-like nitrogen-doped graphene/sulfur composite for lithium-sulfur batteries with enhanced rate performance *J. Alloy. Compd.* **753** 622–9

[26] Zhao X, Kim M, Liu Y, Ahn H J, Kim K W, Cho K K and Ahn J H 2018 Root-like porous carbon nanofibers with high sulfur loading enabling superior areal capacity of lithium sulfur batteries *Carbon* **128** 138–46

[27] Burdzik A, Staehler M, Carmo M and Stolten D 2018 Impact of reference values used for surface free energy determination: an uncertainty analysis *Int. J. Adhes.* **82** 1–7

[28] Davoodabadi A, Li J, Liang Y, Wang R, Zhou H, Wood D L, Singler T J and Jin C 2018 Characterization of surface free energy of composite electrodes for lithium-ion batteries *J. Electrochem. Soc.* **165** A2493–501

[29] Su R and Zhang X 2018 Wettability and surface free energy analyses of monolayer graphene *J. Therm. Sci.* **27** 359–63

[30] Li Z, Li C, Ge X, Ma J, Zhang Z, Li Q, Wang C and Yin L 2016 Reduced graphene oxide wrapped MOFs-derived cobalt-doped porous carbon polyhedrons as sulfur

immobilizers as cathodes for high performance lithium sulfur batteries *Nano Energy* **23** 15–26

[31] Dong Y, Liu S, Wang Z, Liu Y, Zhao Z and Qiu J 2015 Sulfur-infiltrated graphene-backboned mesoporous carbon nanosheets with a conductive polymer coating for long-life lithium-sulfur batteries *Nanoscale* **7** 7569–73

[32] Li F, Kaiser M R, Ma J, Guo Z, Liu H and Wang J 2018 Free-standing sulfur-polypyrrole cathode in conjunction with polypyrrole-coated separator for flexible Li-S batteries *Energy Storage Mater.* **13** 312–22

[33] Chen M, Wang X, Cai S, Ma Z, Song P and Fisher A C 2016 Enhancing the performance of lithium-sulfur batteries by anchoring polar polymers on the surface of sulfur host materials *J. Mater. Chem.* A **4** 16148–56

[34] Zu C, Su Y S, Fu Y and Manthiram A 2013 Improved lithium-sulfur cells with a treated carbon paper interlayer *Phys. Chem. Chem. Phys.* **15** 2291–7

[35] Shao B and Taniguchi I 2014 Synthesis of Li_2MnSiO_4/C nanocomposites for lithium battery cathode employing sucrose as carbon source *Electrochim. Acta* **128** 156–62

[36] Chen T, Zhang Z, Cheng B, Chen R, Hu Y, Ma L, Zhu G, Liu J and Jin Z 2017 Self-templated formation of interlaced carbon nanotubes threaded hollow Co_3S_4 nanoboxes for high-rate and heat-resistant lithium-sulfur batteries *J. Am. Chem. Soc.* **139** 12710–5

[37] Li Z, Wu H B and Lou X W 2016 Rational designs and engineering of hollow micro-/nanostructures as sulfur hosts for advanced lithium-sulfur batteries *Energy Environ. Sci.* **9** 3061–70

[38] Zhou J, Lin N, Cai W L, Guo C, Zhang K, Zhou J, Zhu Y and Qian Y 2016 Synthesis of S/CoS_2 nanoparticles-embedded N-doped carbon polyhedrons from polyhedrons ZIF-67 and their properties in lithium-sulfur batteries *Electrochim. Acta* **218** 243–51

[39] Bao W, Zhang Z, Qu Y, Zhou C, Wang X and Li J 2014 Confine sulfur in mesoporous metal-organic framework@reduced graphene oxide for lithium sulfur battery *J. Alloy. Compd.* **582** 334–40

[40] Zeng P, Huang L, Zhang X, Zhang R, Wu L and Chen Y 2018 Long-life and high-areal-capacity lithium-sulfur batteries realized by a honeycomb-like N, P dual-doped carbon modified separator *Chem. Eng. J.* **349** 327–37

[41] Li H H, Wu X L, Sun H Z, Wang K, Fan C Y, Zhang L L, Yang F M and Zhang J P 2015 Dual-porosity SiO_2/C

nanocomposite with enhanced lithium storage performance *J. Phys. Chem.* C **119** 3495–501

[42] Fan M, An Y, Yin H, Li W, Sun W and Lin Z 2018 Self-assembled reduced graphene oxide/sulfur composite encapsulated by polyaniline for enhanced electrochemistry performance *J. Solid State Electr.* **22** 667–75

[43] Jing H K, Kong L L, Liu S, Li G R and Gao X P 2015 Protected lithium anode with porous Al_2O_3 layer for lithium-sulfur battery *J. Mater. Chem.* A **3** 12213–9

[44] Yao Y, Liu P, Zhang Q, Zeng S, Chen S, Zou G, Zou J, Zeng X and Li X 2018 Nitrogen-doped micropores binder-free carbon-sulphur composites as the cathode for long-life lithium-sulphur batteries *Mater. Lett.* **231** 159–62

[45] You Y, Ye Y, Wei M, Sun W, Tang Q, Zhang J, Chen X, Li H and Xu J 2019 Three-dimensional MoS_2/rGO foams as efficient sulfur hosts for high-performance lithium-sulfur batteries *Chem. Eng. J.* **355** 671–8

[46] Yang W, Yang W, Feng J and Qin X 2018 A polypyrrole-coated acetylene black/sulfur composite cathode material for lithium-sulfur batteries *J. Energy Chem.* **27** 813–9

[47] Wei W, Du P, Liu D, Wang Q and Liu P 2018 Facile one-pot synthesis of well-defined coaxial sulfur/polypyrrole tubular nanocomposites as cathodes for long-cycling lithium-sulfur batteries *Nanoscale* **10** 13037–44

[48] Sun F, Wang J, Chen H, Li W, Qiao W, Long D and Ling L 2013 High efficiency immobilization of sulfur on nitrogen-enriched mesoporous carbons for Li-S batteries *ACS. Appl. Mater. Inter.* **5** 5630–8

[49] Li D, Han F, Wang S, Cheng F, Sun Q and Li W C 2013 High sulfur loading cathodes fabricated using peapodlike, large pore volume mesoporous carbon for lithium-sulfur battery *ACS. Appl. Mater. Inter.* **5** 2208–13

[50] Wang J, Polleux J, Lim J and Dunn B 2007 Pseudocapacitive contributions to electrochemical energy storage in TiO_2 (anatase) nanoparticles *J. Phys. Chem.* C **111** 14925–31

[51] Hu X, Li Y, Zeng G, Jia J, Zhan H and Wen Z 2018 Three-dimensional network architecture with hybrid nanocarbon composites supporting few-layer MoS_2 for lithium and sodium storage *ACS Nano* **12** 1592–602

[52] Tian W *et al* 2018 Metal-organic frameworks mediated synthesis of one-dimensional molybdenum-based/carbon composites for enhanced lithium storage *ACS Nano* **12** 1990–2000